JACS
JOURNAL OF THE AMERICAN CHEMICAL SOCIETY
Article
pubs.acs.org/JACS

Influence of the Donor Size in D−π−A Organic Dyes for Dye-Sensitized Solar Cells

Jiabao Yang,[†,‡] Paramaguru Ganesan,[‡] Joël Teuscher,[‡] Thomas Moehl,[‡] Yong Joo Kim,[‡,§] Chenyi Yi,[‡] Pascal Comte,[‡] Kai Pei,[†] Thomas W. Holcombe,[‡] Mohammad Khaja Nazeeruddin,[‡] Jianli Hua,*[,†] Shaik M. Zakeeruddin,*[,‡] He Tian,[†] and Michael Grätzel*[,‡]

[†]Key Laboratory for Advanced Materials and Institute of Fine Chemicals, East China University of Science and Technology, Shanghai 200237, People's Republic of China

[‡]Laboratory of Photonics and Interfaces, Institute of Chemical Sciences and Engineering, Ecole Polytechnique Fédérale de Lausanne, CH-1015 Lausanne, Switzerland

[§]R & D Center DSC Team, Dongjin Semichem Co., Ltd., 445-935 Hwasung, South Korea

Supporting Information

ABSTRACT: We report two new molecularly engineered push−pull dyes, i.e., **YA421** and **YA422**, based on substituted quinoxaline as a π-conjugating linker and bulky-indoline moiety as donor and compared with reported **IQ4** dye. Benefitting from increased steric hindrance with the introduction of bis(2,4-dihexyloxy)benzene substitution on the quinoxaline, the electron recombination between redox electrolyte and the TiO_2 surface is reduced, especially in redox electrolyte employing Co(II/III) complexes as redox shuttles. It was found that the open circuit photovoltages of **IQ4**, **YA421**, and **YA422** devices with cobalt-based electrolyte are higher than those with iodide/triiodide electrolyte by 34, 62, and 135 mV, respectively. Moreover, the cells employing graphene nanoplatelets on top of gold spattered film as a counter electrode (CE) show lower charge-transfer resistance compared to platinum as a CE. Consequently, **YA422** devices deliver the best power conversion efficiency due to higher fill factor, reaching 10.65% at AM 1.5 simulated sunlight. Electrochemical impedance spectroscopy and transient absorption spectroscopy analysis were performed to understand the electrolyte influence on the device performances with different counter electrode materials and donor structures of donor−π−acceptor dyes. Laser flash photolysis experiments indicate that even though the dye regeneration of **YA422** is slower than that of the other two dyes, the slower back electron transfer of **YA422** contributes to the higher device performance.

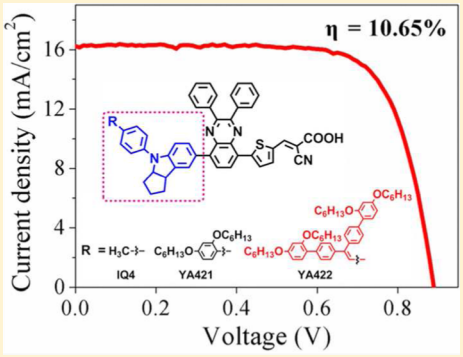

1. INTRODUCTION

Significant attention has been attracted by dye-sensitized solar cells (DSSCs) as alternatives to traditional solar cells, owing to their low-cost fabrication combined with high solar energy to electricity power conversion efficiency (PCE).[1,2] The performance of DSSCs depends on the nature of sensitizer(s), photoanode, counter electrode, and electrolyte and their combination.[3] It is necessary to utilize dyes that possess broad absorption spectra to absorb more photons of sunlight for efficient solar energy to electricity conversion. Ruthenium sensitizer-based DSSCs in combination with volatile electrolyte and platinum counter electrodes show a certified PCE value of 11.9%.[4−7] At the same time, the research activity has increased in finding ruthenium-free sensitizers recently, as ruthenium is a noble and expensive metal. Metal-free organic sensitizers have a number of advantages, such as high molar extinction coefficient, good flexibility of molecular tailoring, tunable spectral properties, relatively high efficiency, and low cost.[8−13] In general, most organic sensitizers are synthesized with the donor−π−acceptor (D−π−A) configuration, due to the efficient intramolecular charge transfer (ICT) properties of this class of molecules.[14,15] Based on this strategy, a series of novel donor−acceptor−π−acceptor (D−A−π−A) organic dyes incorporating internal electron-withdrawing units such as diketopyrrolopyrrole,[16−19] bithiazole,[20,21] isoindigo,[22] benzothiadiazole,[10,15,23] benzotriazole,[24] and quinoxaline[25−27] into the traditional D−π−A structure were reported to extend further the spectral response. Among the nonruthenium-based sensitizers, a donor−acceptor zinc-porphyrin cosensitized DSSC in combination with a cobalt-based electrolyte obtained a new PCE record of 12.3%.[28]

In terms of electrolyte development for the high DSSC device performance, cobalt polypyridyl-based electrolytes have an edge over the other redox electrolytes due to the feasibility of easily tuning the redox energy of electrolytes by varying the structure of the polypyridyl ligands.[29] The main advantage of cobalt-based redox electrolytes lies in obtaining higher device open-circuit photovoltage (V_{oc}) values by tuning the redox

Received: January 10, 2014
Published: March 24, 2014

   dx.doi.org/10.1021/ja500280r | J. Am. Chem. Soc. 2014, 136, 5722−5730

energy of the electrolytes and reducing the excess regeneration energy losses.[30] Redox energy tuning is not possible with traditional iodide/triiodide-based redox electrolytes, as the redox energy of the electrolyte is almost fixed. However, one of the disadvantages of the cobalt-based electrolyte compared to iodide/triiodide redox electrolyte is its faster recombination kinetics with the injected electrons in the TiO_2 film due to its one-electron charge-transfer (CT) mechanism. Faster interfacial charge recombination will lower the open circuit photovoltage (V_{oc}) and reduce the charge collection efficiency, thus decrease the short-circuit photocurrent density (J_{sc}) and the power conversion efficiency (PCE).[31] Evidence from recent research suggests that the introduction of long alkyl chain groups into dye structure can effectively control the unwanted recombination process.[32] Inspired by the performance of quinoxaline dye **IQ4**[27] employing iodide electrolyte and to make an efficient use of the one-electron transfer cobalt redox electrolyte, we introduced different size bulky donor moieties into D−π−A organic sensitizers (**YA421** and **YA422**, as shown in Figure 1) to protect the approach of redox electrolyte closer

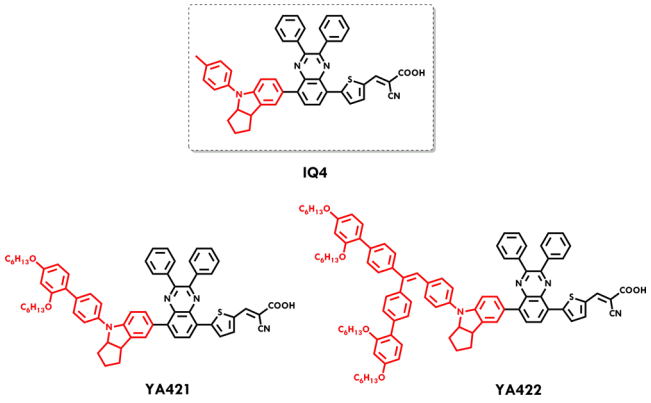

Figure 1. Molecular structures of quinoxaline-based dyes.

to the surface of TiO_2 film. Two newly developed dyes were investigated with cobalt and iodide-based electrolytes and compared with **IQ4** dye to understand the donor size influence on the device performance. The **YA422**-based DSSC with the biggest donor group performed worst with iodide-based electrolyte, but it was the best with cobalt-based electrolyte. Further optimization of **YA422**-based DSSC with different counter electrodes (graphene nanoplatelets and gold/graphene nanoplatelets instead of conventional platinum) and cobalt-based electrolyte yielded the highest device PCE of 10.65% at full sunlight intensity. To the best of our knowledge, this is the highest PCE ever reported by employing a single metal-free sensitizer. Electrochemical impedance spectroscopy (EIS) and transient absorbance spectroscopy (TAS) analysis were performed to understand the influence of electrolyte and counter electrode on the dye regeneration and recombination kinetics of DSSC devices.

2. RESULTS AND DISCUSSION

2.1. Synthesis. Compared to the small indoline as a donor of **IQ4** dye, the uniqueness of the bigger indoline donor lies in the additional bis(2,4-dialkoxy)benzene substituents to terminate the indoline unit, which not only improve their solubility but also decrease electron recombination and thus increase the open circuit voltage, especially in the presence of cobalt electrolyte.[33] The synthetic route to the dyes **YA421** and **YA422** containing quinoxaline moiety is depicted in Scheme 1.

Scheme 1. Synthetic Procedure of the Dyes YA421 and YA422

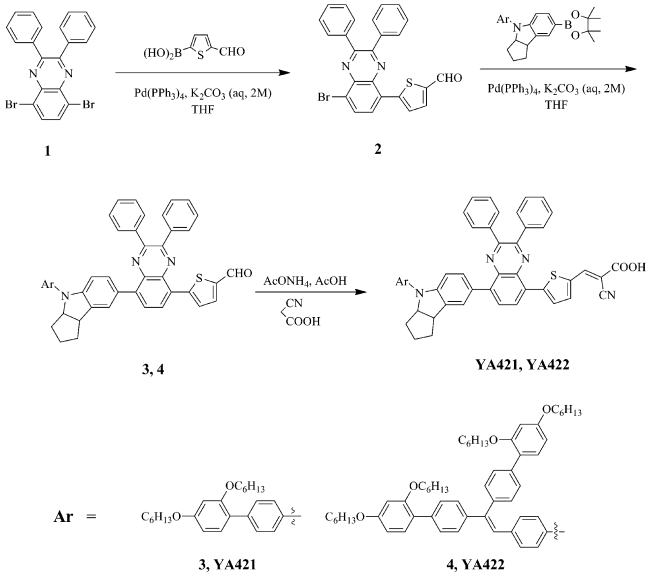

Suzuki coupling reaction of 5,8-dibromo-2,3-diphenylquinoxaline (**1**) with (5-formylthiophen-2-yl)boronic acid gave monoaldehyde-substituted compound **2**. In the next step, Suzuki coupling of **2** with two different indoline boronic acid pinacol esters afforded **3** and **4**, respectively. Finally, the target products (**YA421** and **YA422**) were obtained via Knoevenagel condensation reaction of the respective two aldehydes with cyanoacetic acid in the presence of ammonium acetate. All the intermediates and target dyes were fully confirmed by ^{1}H NMR, ^{13}C NMR, and HRMS (see the Supporting Information).

2.2. Optical Properties. The absorption spectra of **IQ4**, **YA421**, and **YA422** in dichloromethane (DCM) solution are shown in Figure 2. The extension of the π-system of the

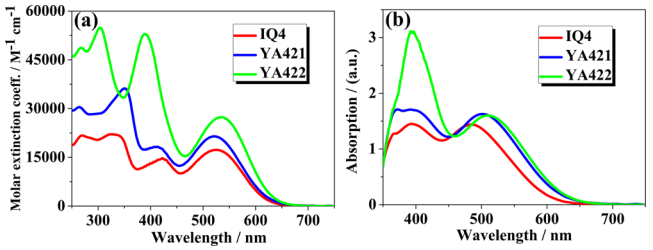

Figure 2. UV−vis absorption spectra of **IQ4**, **YA421**, and **YA422** in DCM solution (a) and adsorbed on 4 μm transparent TiO_2 films (b).

electron-donating moiety does not lead to significant changes in the position of the lowest energy absorption band but has a stronger influence on higher energy absorption band. For all the three dyes, the lowest energy absorption peak is around 522−534 nm. The absorption band positions and their relative intensities are tabulated in Table 1. Obviously, the insertion of the additional phenyl units and extending the donor part of **YA422** leads to increased intensity of the high energy bands with a blue shift in the spectral response, which is assigned to π−π* CT transitions of the donor moiety. The shorter

dx.doi.org/10.1021/ja500280r | J. Am. Chem. Soc. 2014, 136, 5722−5730

Table 1. Photophysical and Electrochemical Properties of Dyes

dye	λ_{max},[a] nm ($\varepsilon \times 10^{-4}$ M cm)	λ_{max},[b] nm	amount, 10^{-8} (mol cm^{-2})	E^0_{ox},[c] V (vs NHE)	E_{0-0},[d] V	$\Phi^0(S^+/S^*)$,[e] V (vs NHE)
IQ4	526 (1.73), 423 (1.47)	487	8.35	0.96	1.97	−1.01
YA421	522 (2.14), 413 (1.83)	502	7.61	0.95	1.94	−0.99
YA422	534 (2.74), 388 (5.30)	508	5.85	0.94	1.91	−0.97

[a]Absorption maximum in DCM at room temperature. [b]Absorption maximum on 4 μm transparent TiO_2 films (cosensitized with 10 mM CDCA). [c]Redox potentials were measured in DCM with 0.1 M tetrabutylammonium hexafluorophosphate ($TBAPF_6$) as electrolyte (working electrode: glassy carbon; reference electrode: Pt; counter electrode: Pt; calibrated with ferrocene/ferrocenium (Fc/Fc^+) as an internal reference and converted to NHE by addition of 0.69 V). [d]E_{0-0} was estimated from the absorption thresholds from absorption spectra of dyes in solution. [e]$\Phi^0(S^+/S^*)$ is estimated by subtracting E_{0-0} to E^0_{ox}.

Table 2. Photovoltaic Performance of the DSSCs Based on IQ4, YA421, and YA422[a]

dye	electrolyte	J_{sc} (mA cm^{-2})	V_{oc} (mV)	FF	η (%)
IQ4	$[Co(bpy)_3]^{2+/3+}$	14.69 (14.44 ± 0.25)	771 (775 ± 4)	0.688 (0.706 ± 0.018)	7.79 (7.90 ± 0.11)
YA421	$[Co(bpy)_3]^{2+/3+}$	15.76 (15.46 ± 0.30)	803 (804 ± 1)	0.712 (0.717 ± 0.005)	9.00 (8.91 ± 0.09)
YA422	$[Co(bpy)_3]^{2+/3+}$	15.26 (15.34 ± 0.08)	876 (853 ± 23)	0.689 (0.702 ± 0.013)	9.22 (9.18 ± 0.04)
IQ4	I^-/I_3^-	15.33 (15.51 ± 0.18)	737 (730 ± 8)	0.755 (0.758 ± 0.003)	8.53 (8.60 ± 0.07)
YA421	I^-/I_3^-	15.41 (15.08 ± 0.33)	741 (744 ± 3)	0.711 (0.728 ± 0.017)	8.12 (8.16 ± 0.04)
YA422	I^-/I_3^-	14.40 (14.44 ± 0.04)	741 (743 ± 2)	0.682 (0.686 ± 0.004)	7.28 (7.36 ± 0.08)

[a]Measured under irradiation of AM 1.5 simulated solar light (100 mW cm^{-2}) at room temperature, iodide electrolyte containing: 1.0 M 1,3-dimethylimidazolium iodide, 0.03 M iodine, 0.1 M guanidinium thiocyanate, 0.5 M *tert*-butylpyridine, 0.05 M lithium iodide in acetonitrile:valeronitrile (85:15, v/v), cobalt electrolyte containing: 0.22 M $Co(bpy)_3[B(CN)_4]_2$, 0.06 M $Co(bpy)_3[B(CN)_4]_3$, 0.1 M $LiClO_4$, and 0.5 M 4-*tert*-butylpyridine in acetonitrile; the concentration of dyes is 3×10^{-4} M in chloroform/ethanol (v/v: 3/7) mixed solvent with 10 mM CDCA, platinum is the counter electrode. Double-layer TiO_2 film (4 + 4 μm) was used with active area of 0.159 cm^2. Average values are based on two replicate measurements.

wavelength absorption band (360−440 nm) corresponds to quinoxaline moieties as a spacer. The dyes **YA421** and **YA422** adsorbed on 4 μm transparent TiO_2 films (Figure 2b) show advantage over the **IQ4** dye being red-shifted in the spectral response. The blue shift in the absorption spectra of dyes adsorbed on the surface of TiO_2 film compared to the absorption spectra in solution (39, 20, and 26 nm for **IQ4**, **YA421** and **YA422**, respectively) might be ascribed to the deprotonation of the carboxylic acid.[34]

2.3. Electrochemical Properties. The redox potentials of **IQ4**, **YA421**, and **YA422** dyes, measured by cyclic voltammetry (CV), are shown in Figure S1, and the values are presented in Table 1. The redox potentials of the **IQ4**, **YA421** and **YA422** are 0.96, 0.95, and 0.94 V vs NHE, respectively, which are higher than that of the iodide/triiodide (0.40 V vs NHE) or $Co(bpy)_3^{2+/3+}$ (0.57 V vs NHE)[31] redox electrolyte energy level, guaranteeing ample driving force for the dye regeneration. The structural differences in the donor part of **IQ4**, **YA421**, and **YA422** have little influence on their redox potentials. By extending the donor conjugation of **YA422**, the redox potential is increased by 20 mV compared to **IQ4**. Estimated from the absorption thresholds from absorption spectra of dyes in solution, the zero−zero transition energies (E_{0-0}) were determined to be 1.97, 1.94, and 1.91 V, respectively. The excited-state reduction potentials of **IQ4**, **YA421**, and **YA422** were obtained by combining the redox potentials with the energy of the transition (E_{0-0}). The calculated excited-state potentials of these dyes (−1.01, −0.99, and −0.97 V, respectively) are placed sufficiently above the TiO_2 conduction band edge to ensure no energetic barriers for the electron injection.

2.4. Photovoltaic Performance of DSSCs. The photovoltaic performance of devices with **IQ4**, **YA421**, and **YA422** dyes was investigated using double-layer TiO_2 films as photo anodes (4 μm transparent TiO_2 layer and 4 μm TiO_2 scattering layer) in combination with platinum (Pt) as a counter electrode (CE), and the photovoltaic parameters are presented in Table 2. The photocurrent−voltage curve as well the incident photon to current conversion efficiency (IPCE) value of the **IQ4**, **YA421**, and **YA422** dyes containing DSSC devices are shown in Figure S2. All of the IPCEs do not show great difference due to their similar absorption spectra and energy levels. For the iodide-based electrolyte, the devices with **IQ4**, **YA421**, and **YA422** dyes show similar V_{oc} values, whereas the FF and PCE decreases in the trend of **YA422** > **YA421** > **IQ4**. Due to the smaller size of triiodide spicies compared to Co^{3+} complex the introduction of long alkyl chains has less influence in retarding the recombination in the iodide/triiodide redox electrolyte-based devices (see Section 2.5, Electrochemical Impedance Analysis). The best PCE of 8.53% was obtained with **IQ4** in AM 1.5 simulated solar light (100 mW cm^{-2}). It is interesting to note that the device performance trend with cobalt-based electrolyte is just opposite to the trend that obtained with iodide-based electrolyte. In case of cobalt-based electrolytes, the IPCE values of **YA421** and **YA422** reached a value of 90% at 550 nm, whereas a maximum of 80% is reached for **IQ4** devices. The V_{oc} and PCE of the devices increased in the order of **YA422** > **YA421** > **IQ4.** The lower light harvesting capability of **IQ4** device (as shown in the Figure S2a) might be responsible for the lower J_{sc} obtained for **IQ4** devices than that of **YA421** and **YA422** devices. Another reason for the lower J_{sc} of **IQ4** devices with cobalt-based electrolyte than that of iodide-based electrolyte could be due to the faster electron recombination of injected electrons from the TiO_2 to the electrolyte. It is known that the electron recombination with one electron-transfer cobalt redox electrolyte is more facile than that with two-electron-transfer iodide-based electrolyte.[35] However, in case of **YA421** and **YA422** dyes the presence of bulky donor groups (containing long alkoxy chains) shields the approach of cobalt complexes closer to TiO_2 surface more effectively due to their relatively bigger size of cobalt complex compared to iodide/triiodide molecules. The decreased

dx.doi.org/10.1021/ja500280r | J. Am. Chem. Soc. 2014, 136, 5722−5730

recombination in **YA422**-based device contributes to an increase in the V_{oc} value by more than 100 mV compared to the **IQ4**-based devices. The best performing **YA422** reached 9.22% PCE at full sunlight intensity in combination with Pt counter electrode.

Pt is known as the best catalyst for the regeneration of I^-/I_3^- based electrolyte. However, a number of recent studies show that a carbonaceous type catalyst outperforms Pt with the cobalt redox electrolyte, due to the low CT resistance at the counter electrode.[36,37] The influence of CE material on the device performance was also explored by comparing Pt CE with the graphene nanoplatelets (GNP) CE and the photovoltaic performance at three different light intensities (100%, 50%, and 10%, respectively) are shown in Figure 3, and the data are

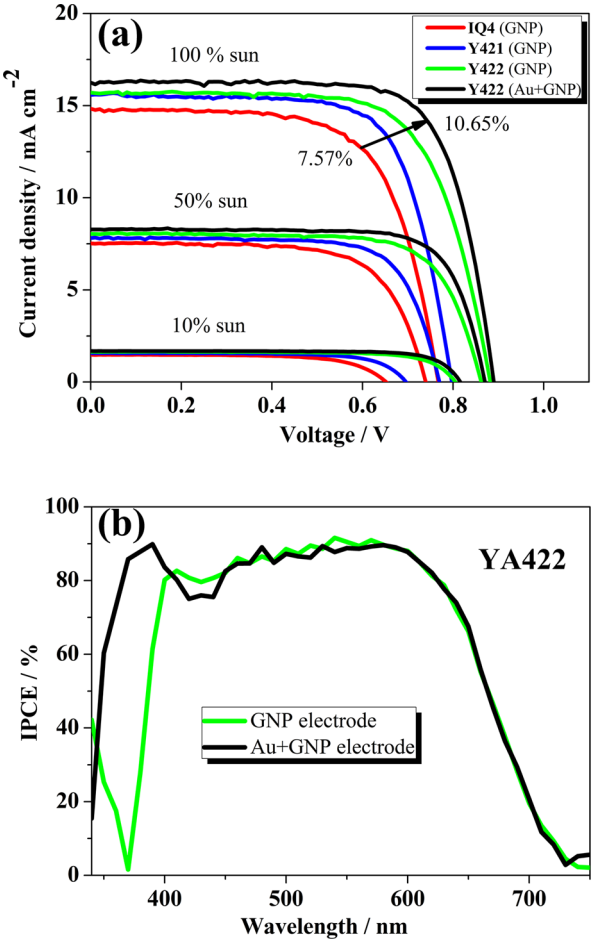

Figure 3. (a) *I*–*V* curves for DSSCs based on dyes **IQ4**, **YA421**, **YA422** using GNP counter electrode and **YA422** using Au-sputtered GNP counter electrode. (b) IPCE curves for DSSCs based on **YA422** employing two different counter electrodes.

presented in Table 3. Applying either Pt or GNP as CE there is no difference in the PCE trend (**YA422** > **YA421** > **IQ4**) of the devices. Interestingly, in spite of lower fill factor (FF) values obtained with GNP CE, the **YA422** device PCE reached 9.60% at full sunlight intensity. There is a possibility to increase the PCE further by improving the FF value of device. Instead of depositing the graphene nanoplatelets on FTO glass to produce the CE, a sputtered gold layer (50 nm) was deposited on FTO glass, which can be beneficial not only to reflect back the sunlight at the CE (contributing to increased J_{sc}) but also to decrease the CT resistance at the CE (contributing to increased FF). As far as we know, this is the first time that a gold-sputtered GNP covered CE is applied in DSSCs. For a champion cell applying Au + GNP as the CE, the FF is improved largely and combined with an increase in J_{sc}, and the PCE is enhanced dramatically to 10.65% under full sunlight. At half sunlight intensity, the device performance even reaches to 10.93% PCE. To the best of our knowledge, this is the highest device performance reported for any sole D−π−A metal-free dye.

2.5. Electrochemical Impedance Analysis. To understand the intriguing results obtained with two different redox electrolytes with different CE materials, we applied EIS analysis to get a clear picture on the internal electrical parameters of the devices. The measured dark currents and the results obtained by fitting the EIS measurements using the transmission line model[38−40] are presented in the Figure S3. The apparent electron lifetime (τ_n) and transport time (τ_{trans}) have been calculated by using the transport (R_{trans}) and recombination (R_{ct}) resistance in conjunction with the chemical capacitance (C_{chem}) of the TiO_2 ($\tau_n = R_{ct} \times C_{chem}$ and $\tau_{trans} = R_{trans} \times C_{chem}$).[38−40] The iodide electrolyte-based devices show a comparable τ_n for the dyes **YA421** and **YA422** and a slightly lower τ_n for the **IQ4**, in accordance with their attained V_{oc} values (Figure 4A and Table 2). There is a minor shift in the TiO_2 conduction band edge position (E_{cb}) of the devices (Figure S3C) as noticed in the chemical capacitances (about 15 mV from high to low E_{cb}: **IQ4** to **YA422** to **YA421**). This is compensated by the increased τ_n value of **YA422** and **YA421**. The variations in the FF can be explained by looking at the counter electrode and the Warburg diffusion resistance (Figure S4). The **IQ4** device shows the highest FF followed by **YA421** and **YA422** devices since the highest Warburg diffusion resistance is observed for **YA422**, while the highest CE resistance is measured for **YA421**. The differences in J_{sc} cannot be conclusively explained by EIS experiments as these measurements were done under dark current conditions.

In the case of cobalt redox electrolyte devices, the observed very small difference in the E_{cb} position of the mesoporous TiO_2 for the devices with the different dyes emphasizes that the increases in the V_{oc} results from an increase in the electron lifetime (Figure 4B). The V_{oc} difference between **IQ4** and **YA421** is ∼30 mV and between **YA421** and **YA422** it is ∼70 mV. The τ_n values are in good agreement with the observed device V_{oc} values (a rough estimate from the diode equation $\Delta V_{oc} = (k_B T/q)(\ln(\tau_{n,dye1}/\tau_{n,dye2})$ with k_B as Boltzmann constant, q as elementary charge, and T as temperature leads to a difference of about ΔV_{oc} = 20 mV between **IQ4** and **YA421** and ΔV_{oc} = 68 mV **YA421**and **YA422**). The bulkier donor part of the dye shields the TiO_2 interface in a better way from approaching of the oxidized species of the redox electrolyte thus reducing the recombination rate. The concept of protecting the TiO_2 surface by the bulkier donor groups with the cobalt-based redox electrolyte has been reported earlier.[32,41] The higher Warburg diffusion resistance of **IQ4** (Figures 5 and S5) is responsible for the lower FF, whereas the higher counter electrode resistance of **YA422** compared to **YA421** is contributing to its lower FF values.

The champion cell fabricated with **YA422** in combination with Au + GNP-based CE yielded the highest PCE of 10.65% due to the best FF and J_{sc} values. In this device, an increase in J_{sc} compared to GNP CE is most probably due to an enhanced back-light reflection from the CE (enabling higher light

dx.doi.org/10.1021/ja500280r | J. Am. Chem. Soc. 2014, 136, 5722−5730

Table 3. Photovoltaic Performance of the DSSCs Based on the Three Dyes with GNP Counter Electrode and YA422 with Au + GNP Counter Electrode[a]

dye	CE	I_0 (mW cm^{-2})	J_{sc} (mA cm^{-2})	V_{oc} (mV)	FF	η (%)
IQ4	GNP[b]	100	14.83 (14.66 ± 0.17)	767 (769 ± 2)	0.666 (0.660 ± 0.006)	7.57 (7.44 ± 0.13)
		50	7.52 (7.40 ± 0.12)	739 (741 ± 2)	0.692 (0.687 ± 0.005)	7.70 (7.53 ± 0.17)
		10	1.48 (1.46 ± 0.02)	651 (653 ± 2)	0.672 (0.673 ± 0.001)	6.45 (6.42 ± 0.03)
YA421	GNP[b]	100	15.58 (15.55 ± 0.03)	797 (792 ± 5)	0.712 (0.709 ± 0.003)	8.84 (8.73 ± 0.11)
		50	7.81 (7.76 ± 0.05)	770 (765 ± 5)	0.729 (0.728 ± 0.001)	8.77 (8.65 ± 0.12)
		10	1.56 (1.54 ± 0.02)	695 (691 ± 4)	0.717 (0.712 ± 0.005)	7.78 (7.61 ± 0.17)
YA422	GNP[c]	100	15.71 (15.70 ± 0.62)	882 (868 ± 17)	0.693 (0.698 ± 0.016)	9.60 (9.45 ± 0.45)
		50	8.03 (8.04 ± 0.34)	862 (845 ± 17)	0.730 (0.728 ± 0.011)	10.11 (9.85 ± 0.64)
		10	1.64(1.63 ± 0.06)	805 (780 ± 25)	0.742 (0.746 ± 0.023)	9.86 (9.68 ± 0.47)
	Au + GNP[b]	100	16.25 (16.36 ± 0.11)	890 (887 ± 3)	0.737 (0.732 ± 0.005)	10.65 (10.62 ± 0.03)
		50	8.28 (8.23 ± 0.05)	870 (867 ± 3)	0.759 (0.756 ± 0.003)	10.93 (10.80 ± 0.13)
		10	1.68 (1.72 ± 0.04)	815 (811 ± 4)	0.779 (0.752 ± 0.27)	10.69 (10.32 ± 0.37)

[a]Measured at room temperature, 0.159 cm^2 working area, electrolyte containing: 0.22 M $Co(bpy)_3[B(CN)_4]_2$, 0.06 M $Co(bpy)_3[B(CN)_4]_3$, 0.1 M $LiClO_4$, and 0.5 M 4-*tert*-butylpyridine in acetonitrile, the concentration of dyes is 0.3 mM in chloroform/ethanol (v/v: 3/7) mixed solvent with 10 mM CDCA, the thickness of TiO_2 film is 4 + 4 μm. [b]Average values are based on two replicate measurements. [c]Average values are based on 14 replicate measurements.

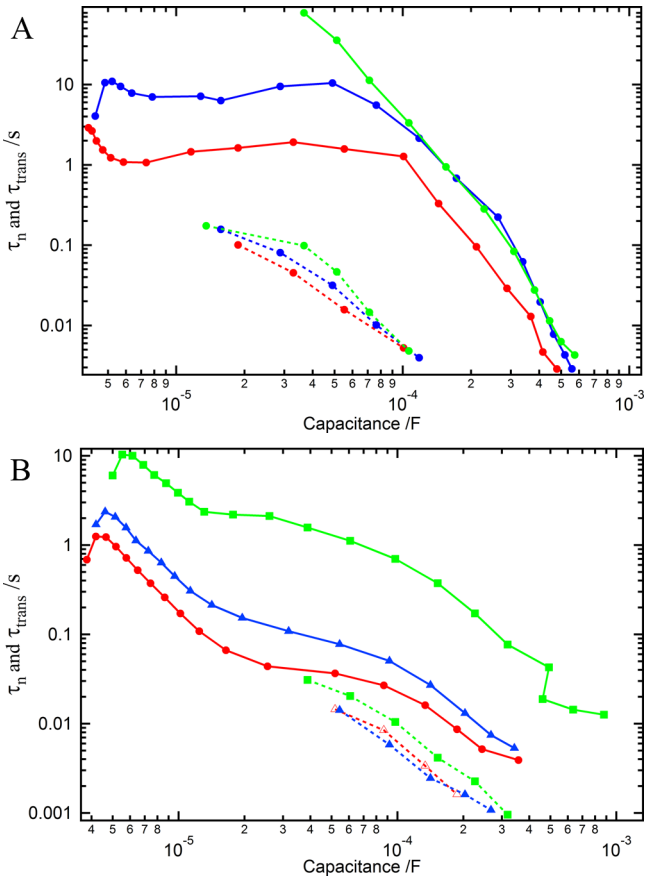

Figure 4. Electron lifetime (solid) and electron transport time (dotted) determined from EIS measurements for the dyes **IQ4** (red), **YA421** (blue), and **YA422** (green). (A) Iodine redox system-based devices; (B) cobalt redox system-based devices with GNP CEs.

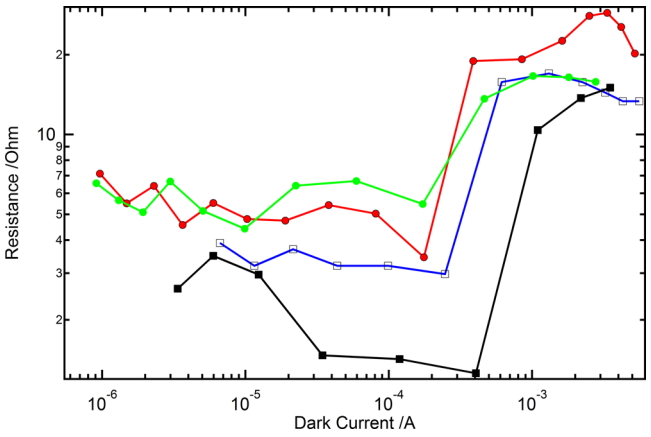

Figure 5. Sum of the series resistance originating from the counter electrode and the Warburg diffusion resistance plotted against the passed dark current for the dyes **IQ4** (red), **YA421** (blue) and **YA422** (green) with cobalt redox system based devices. Black represents the resistance of the device with Au + GNP CE.

harvesting mainly in the wavelength region between 300 and 400 nm), while the FF increase can be evidently assigned to the reduced total series resistance as shown in Figure 5.

2.6. Photoinduced Charge-Transfer Dynamics. Femtosecond pump−probe spectroscopy is used to identify electron injection in the semiconductor. At first, we measured the transient absorbance of dyes adsorbed on insulating alumina films allowing observation of spectral changes due to the formation of dye excited state (see SI for details and Figure S7−S9).

The situation is different if the dyes are adsorbed on the titania film (Figure 6). The excited dye injects an electron into the titania conduction band, and then the molar extinction of excited state (ε^{S*}) is mixed with oxidized dye (ε^{S+}) spectra. On TiO_2 film, the maximum of the transient absorbance is slightly shifted toward the red at 480 nm, and this shift might be due to the differences in the substrate materials (titania or alumina) inducing different electronic environment on the dye. This spectral shift might also arise from the differences in the spectral shape of the excited and oxidized forms of the dye and therefore would reveal some ultrafast electron injection during the initial excitation (<100 fs). Unfortunately, even at the shortest times, one cannot see any wavelength dependent dynamics, preventing the unambiguous assignment of different species over the investigated wavelengths. For all the three dyes, the spectral shape is similar (Figures 6, S10 and S11).

For the **IQ4**, **YA421**, and **YA422** dyes adsorbed on the titania film the transients extracted at 480 nm after exciting the

dx.doi.org/10.1021/ja500280r | J. Am. Chem. Soc. 2014, 136, 5722−5730

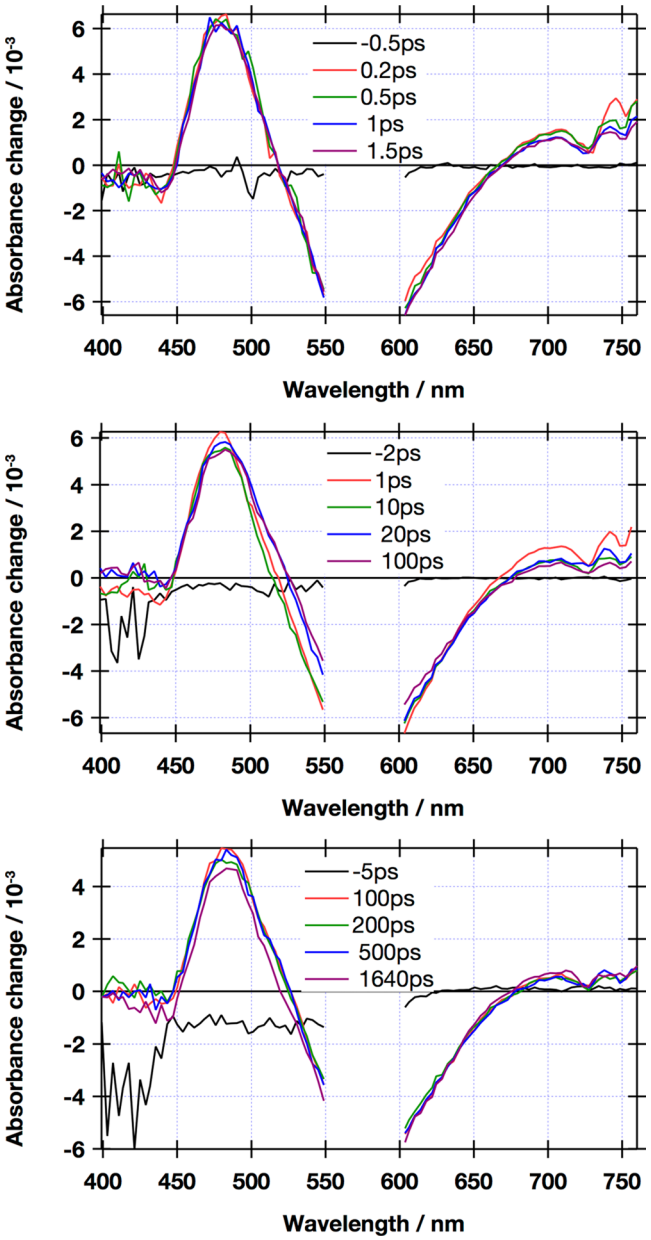

Figure 6. Transient spectra of **YA422** adsorbed on titania and measured in the presence of acetonitrile after excitation at 580 nm. For **IQ4** and **YA421** dyes the data are presented in Figures S10 and S11.

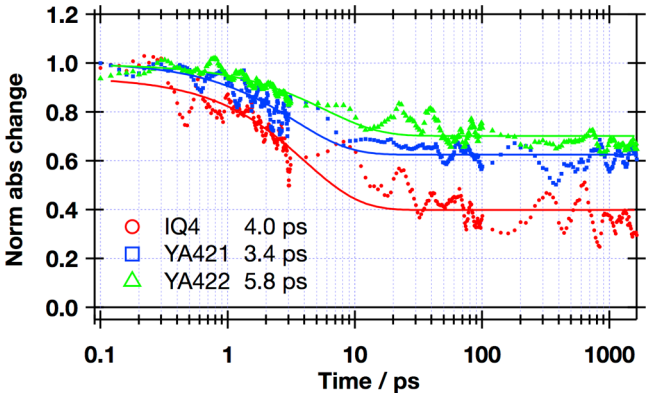

Figure 7. Normalized transient dynamics extracted at 480 nm for **IQ4**, **YA421**, and **YA422** adsorbed on TiO_2 film after exiting at 580 nm in presence of acetonitrile solution. Data are smoothed, and solid lines are the result of a monoexponential fit.

dye at 580 nm are presented in Figure 7. Even having a similar spectral shape, dynamics for titania films are different to that observed on alumina. A first rapid decrease is observed on TiO_2, followed by a plateau over the investigated time scale (1.6 ns), assigned to the oxidized state for the three dyes. This indicates that a difference between ε^{S+} and ε^{S*} allows us for monitoring electron injection at this wavelength. We excluded the influence of a Stark signal at this wavelength thanks to the absence of positive absorbance change in the photoinduced absorption spectroscopy (PIA) spectra (see Figure S6). The transient absorbance spectrum witnessed on alumina samples also supports observation of the excited dye species only. We extracted the electron injection lifetime from a monoexponential fit of the decay with time constants of 4.0, 3.4, and 5.8 ps for **IQ4**, **YA421**, and **YA422**, respectively. At these short time spans, the dye excited-state population did not show a significant decrease on alumina samples (Figure S9), confirming that in this case there is no electron injection. Similar dynamics are found above 700 nm, also thanks to a difference between ε^{S+} and ε^{S*} (1.9, 1.4, 2.2 ps at 700 nm, respectively, see Figure S12). This confirms that the differences in the LUMO levels of these three dyes have negligible influence on the electron injection into the TiO_2 conduction band. The measured time constants for electron injection are significantly slower than the fastest reports for ruthenium dyes,[42] however, the spread of the dynamics is less important and comparable with other reported D−π−A dye results.[43] The observed plateau at longer time period ensures that the oxidized dye is stable over this time scale and that no back electron transfer is occurring. Over the investigated spectral range there is, however, no simple wavelength to extract that would allow to monitor directly either the oxidized dye or its excited state.

To monitor the influence of dye donor group toward the oxidized dye lifetime and its regeneration by electrolytes, nanomicrosecond TAS was applied under open-circuit conditions (Figure 8). After excitation at 535 nm, with a low fluence ensuring on average not more than one electron is injected per nanoparticle, transient decays are monitored at 1100 nm, following the oxidized dye signature found with PIA experiment (see Figure S6). Electrons also absorb at this wavelength, but they have a much smaller extinction coefficient compared to the oxidized dye species.[44] As traces significantly deviate from monoexponential decays, transient absorbance decays are fitted with a stretched exponential to extract back electron transfer and dye regeneration lifetimes.

In the absence of redox active electrolyte such as acetonitrile, oxidized dye has no other pathway than recombining with the injected electrons in TiO_2 film. Thus, following the decay of the oxidized dye allows one to measure the lifetime of the back electron transfer reaction. Oxidized **IQ4** has a lifetime of 438 μs. Increasing the donor size leads to an increase in the lifetime of **YA421** and **YA422** to 595 and 1070 μs, respectively, confirming the hole stabilization by the bigger donor group.

Oxidized dye regeneration occurs in the presence of redox active electrolyte, and therefore a faster decay of dye cation should be present for efficient device performance. For **IQ4**, efficient dye regeneration occurs in the presence of both redox electrolyte types. **YA421** presents faster dye regeneration compared to **YA422** by cobalt-based electrolyte than that of iodide-based electrolyte. The results of the fits and the

dx.doi.org/10.1021/ja500280r | J. Am. Chem. Soc. 2014, 136, 5722−5730

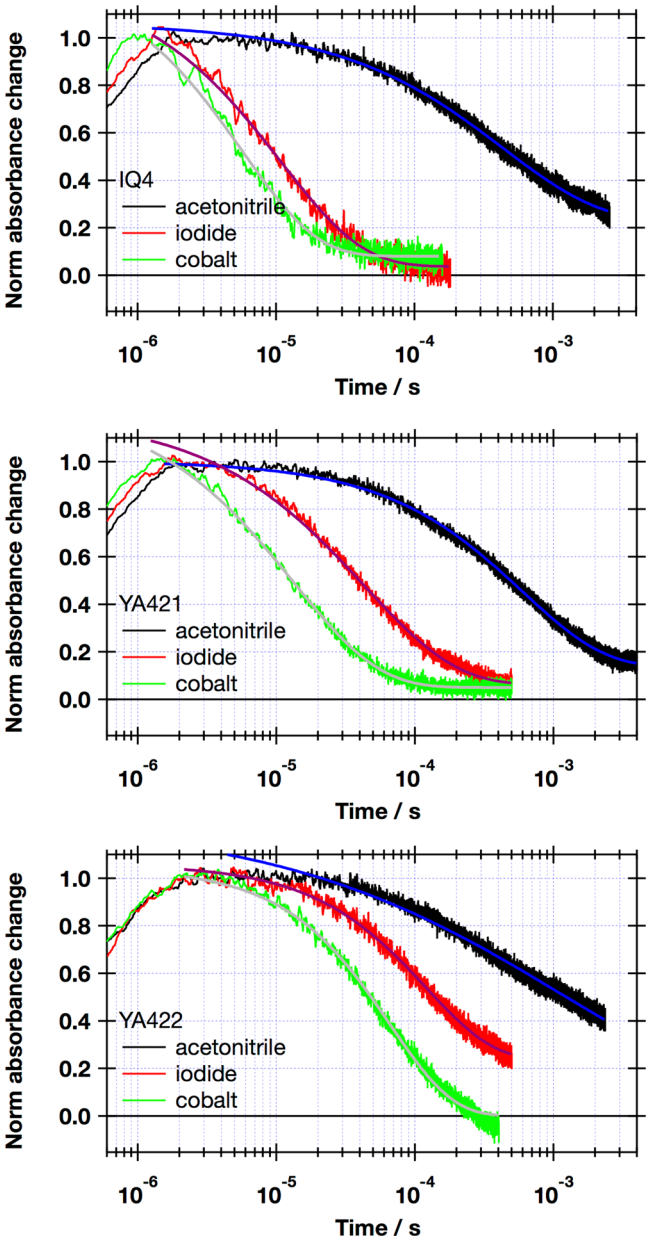

Figure 8. Nanosecond normalized transient absorbance decays of **IQ4**, **YA421**, and **YA422** dyes at 1100 nm in presence/absence of redox electrolyte (iodide or cobalt).

regeneration yields (η_{reg}) are calculated assuming first order rate for dye regeneration and back electron transfer reactions ($\eta_{reg} = k_{reg}/(k_{reg} + k_{rec})$, $k_i = 1/\tau_i$) (in this study, the lifetime extracted from the fit is used as an approximation for τ_i) are summarized in Table 4.[45] This estimation of the regeneration yield might overestimate the true regeneration efficiency according to a recent study.[46]

Table 4. Time Constants Extracted from the Fits of Figure 8 and Calculated Regeneration Yields

	τ_{rec} (μs)	$\tau_{reg\ iodide}$ (μs)	$\eta_{reg\ iodide}$	$\tau_{reg\ cobalt}$ (μs)	$\eta_{reg\ cobalt}$
IQ4	438	10.9	0.98	5.7	0.99
YA421	595	43.2	0.93	13.4	0.98
YA422	1070	120.7	0.90	66.4	0.94

At open-circuit conditions, dye regeneration yields of **IQ4** and **YA421** are close to unity with cobalt-based electrolyte (η_{reg} = 0.99 and 0.98, respectively) and expected to have excellent photovoltaic performance. Whereas in case of iodide-based electrolyte, the dye regeneration yield is lower for **YA421** (η_{reg} = 0.93) than that of **IQ4** (η_{reg} = 0.98). However, the dye regeneration reaction is much slower for **YA422** with both the (iodide or cobalt-based) electrolytes. Fortunately, the long-lived oxidized state of **YA422** is responsible for preventing back electron transfer issues and permits for good dye regeneration yields (η_{reg} = 0.94 and 0.90 for cobalt and iodide electrolytes, respectively) which contributes to excellent device photovoltaic performance. After charge injection, the donor moiety of **YA422** allows for delocalization of the hole further away from the TiO_2 interface. Because of the larger charge separation distance with increasing size of the donor, the trend is similar for the dye regeneration reaction and the back electron transfer reaction, in the presence of both types of electrolyte. This effect is attributed to a steric hindrance of the dye blocking the approach of the redox mediator similarly to what has been observed for ruthenium dyes.[47] The steric hindrance of the dye has same influence in the presence of both the electrolytes that are investigated. As a consequence, dye regeneration reaction lifetime is slowed down by 1 order of magnitude along the dye series for both the electrolytes. The cobalt-based electrolyte involves a one electron dye regeneration reaction compared to two electrons involved in iodide-based electrolyte, and this partly explains the observed differences for the same dye with two different electrolytes.

3. CONCLUSION

We successfully introduced two various degrees of bulky size donors into quinoxaline-based D−π−A dyes as a part of molecular engineering of dyes and to test them in dye-sensitized solar cells. Compared to the reported **IQ4** dye bearing indoline donor, bulky indoline-based dyes **YA421** and **YA422** acquire larger molar extinction coefficient, which is beneficial to apply thinner semiconductor films in DSSCs. It is interesting to note that the photovoltaic performance of all the three dyes studied with Pt as a CE show opposite trend with iodide/triiodide (**IQ4** > **YA421** > **YA422**) and cobalt redox electrolytes (**YA422** > **YA421** > **IQ4**). Electron recombination process was efficiently impeded due to the presence of long alkoxy chains on the bulky donor moieties, particularly with cobalt-based redox electrolyte. For **YA422** dye-containing device, 9.60% PCE was obtained in combination with the GNP CE and cobalt-based electrolyte. Applying Au+GNP as a CE, the FF of **YA422** device increased 6% due to the decrease in the CT resistance at the CE and the J_{sc} increased due to the higher back reflection. Therefore the device performance enhanced to a record efficiency of 10.65%. To the best of our knowledge, this is the highest efficiency reported by a single organic D−π−A dye. Laser flash photolysis experiments indicate that even though the dye regeneration of **YA422** is slower than that of the other two dyes, the slower back electron transfer of **YA422** contributes to the higher device performance. This work emphasizes the significance of the size of the dye in controlling the kinetic parameters, which are responsible in determining the device PCE. Further work will be focused on rational dye design for this system toward red-shifting the dye absorption, giving possibilities to harvest a broader range of photons in the solar spectrum to increase the device performance.

dx.doi.org/10.1021/ja500280r | J. Am. Chem. Soc. 2014, 136, 5722−5730

4. EXPERIMENTAL SECTION

4.1. Materials. Tetra-*n*-butylammonium hexafluorophosphate ($TBAPF_6$), 4-tert-butylpyridine (4-TBP), lithium iodide, and 2-cyanoacetic acid were purchased from Fluka. Starting materials 5,8-dibromo-2,3-diphenylquinoxaline, 4-(2′,4′-bis(hexyloxy)-[1,1′-biphenyl]-4-yl)-7-(4,4,5,5-tetramethyl-1,3,2-dioxaborolan-2-yl)-1,2,3,3a,4,8b-hexahydrocyclopenta[b]indole and 4-(4-(2,2-bis(2′,4′-bis(hexyloxy)-[1,1′-biphenyl]-4-yl)vinyl)phenyl)-7-(4,4,5,5-tetramethyl-1,3,2-dioxaborolan-2-yl)-1,2,3,3a,4,8b-hexahydrocyclopenta[b]indole were synthesized according to the corresponding literature methods.[19,27] $Co(bpy)_3[B(CN)_4]_2$ and $Co(bpy)_3[B(CN)_4]_3$ were prepared in the same manner reported previously.[48] The Thin-layer chromatography (TLC) was conducted with Merck KGaA precoated TLC Silica gel 60 F254 aluminum sheets and visualized with UV and potassium permanganate staining. Flash column chromatography was performed on glass columns packed with silica gel using Silicycle UltraPure SilicaFlash P60, 40−63 mm (230−400 mesh). Graphene nanoplatelets (GNP) were purchased from Cheap Tubes, Inc. (USA, grade 3). All other solvents and chemicals were purchased from Aldrich and used as received without further purification.

4.2. Preparation of the Solar Cells. The dye-sensitized TiO_2 photoelectrode was prepared by following the procedure reported in the literature.[49] The TiO_2 transparent photoelectrodes (4 μm) were prepared by screen-printing onto FTO (fluorine-doped tin oxide, Solar 4 mm thickness, 10 ohms per square, Nippon Sheet Glass) conducting glass. The screen-printing paste was composed of ∼20 nm diameter anatase particles that gave a mesoporous layer with ∼32 nm pores. In order to render high PCE, a scattering layer (4 μm) (400 nm diameter, Catalysts & Chemicals Ind. Co. Ltd. (CCIC), HPW-400) was deposited on the transparent layer. Sintering was carried out at 500 °C for 15 min. The films were soaked in the solution of 0.02 M aqueous $TiCl_4$ for 30 min at 70 °C. After being washed with deionized water and fully rinsed with ethanol, the films were heated again at 500 °C for 15 min. These electrodes were immersed into a 0.3 mM solution of dye with 10 mM 3α,7α-dihydroxy-5β-cholic acid (CDCA) in chloroform/ethanol (3:7 v/v) mixed solvent and kept for 3 h at room temperature. To prepare the counter electrode, a hole (0.8-mm diameter) was drilled on the counter electrode by a Drill-press. For Pt or GNP electrode,[36,37] the Pt or graphene catalyst was deposited on the cleaned FTO glass by coating with four drops of H_2PtCl_6 solution (0.02 M in 2-propanol solution) or GNP solution (1 mg in 1 mL 2-propanol solution) with the heat treatment at 400 °C for 15 min. For Au/GNP electrode, a gold layer (50 nm thick) was deposited on the FTO substrate by a sputter first, and then deposited another graphene layer on the gold electrode with four drops of GNP solution. About the assembly of cells, the dye-contained TiO_2 film and counter electrode were assembled into a sandwich-type cell and sealed with a hot-melt gasket of 25 μm thickness made of the ionomer Surlyn 1702 (Dupont). The redox electrolyte was placed in a drilled hole in the counter electrode, and was driven into the cell by means of vacuum backfilling. The iodide electrolyte consists of 1.0 M 1,3-dimethylimidazolium iodide, 0.03 M iodine, 0.1 M guanidinium thiocyanate, 0.5 M *tert*-butylpyridine, 0.05 M lithium iodide in acetonitrile: valeronitrile (85:15, v/v). The cobalt electrolyte consists of 0.22 M $Co(bpy)_3[B(CN)_4]_2$, 0.06 M $Co(bpy)_3[B(CN)_4]_3$, 0.1 M $LiClO_4$, and 0.5 M 4-tert-butylpyridine in acetonitrile. Finally, the hole was sealed using Surlyn and a cover glass (0.1 mm thickness).

4.3. Photovoltaic Performance Measurements. For photovoltaic measurements of the DSCs, a solar simulator equipped with a 450 W xenon light source (Osram XBO 450) with a filter (Schott 113) was employed, whose power was regulated to the AM 1.5 solar standard by using a reference Si photodiode equipped with a color-matched filter (KG-3, Schott) to reduce the mismatch in the region of 350−750 nm between the simulated light and AM 1.5 to less than 4%. The measurement-settling time between applying a voltage and measuring a current density for the $I-V$ characterization of DSCs was fixed to 80 ms with a Keithley model 2400 digital source meter. The photocurrent action spectra were measured with an Incident Photon-to-Current Conversion Efficiency (IPCE) test system. The modulation frequency used was about 2 Hz and light from a 300 W xenon lamp (ILC Technology, USA) was focused through a computer controlled Gemini-180 double monochromator (John Yvon Ltd., UK). A white light bias (5%) was used to bring the total light intensity on the device under testing closer to operating conditions. A light mask was used on the DSCs, so the illuminated active area of DSCs was fixed to 0.159 cm^2.

4.4. Electrochemical Impedance Spectroscopy (EIS). The EIS analysis was done on DSC devices at room temperature in the dark. A sinusoidal potential perturbation with an amplitude of 15 mV was applied over a frequency range 7 MHz − 0.1 Hz (Bio Logic SP300 potentiostat) at constant potential bias. The bias potential varied between 0 mV and V_{oc} with about 50 mV step. The spectra were fitted using ZView software (Scribner Associates) using the transmission line model.[38−40] If the potential was corrected for the ohmic losses by the series resistance of the devices this is indicated in the figure caption.

4.5. Femtosecond Pump−Probe Spectroscopy. The femtosecond transient spectrometer is based on an amplified Ti:Sapphire femtosecond laser at 1 kHz (CPA-2001, Clark-MXR). It sourced a noncollinear optical parametric amplifier tuned at 580 nm for the pump and a white light continuum generated in a CaF_2 crystal for the probe. Typical instrument response measured by a Kerr gating technique in a thin glass window was 50 fs and spectra were corrected for the temporal chirp of the white light pulse. Probe pulses were delayed with respect to the pump pulses using a computer controlled optical delay line. The probe was detected with a pair of 150 mm spectrographs (SpectraPro-2150, Acton Research Corporation) equipped with 512 × 58 pixels back-thinned CCD detectors (Hamamatsu S7030−0906). The transmitted signal intensity was recorded shot by shot and corrected for fluctuations against a reference beam. 4000 averaged pulses were needed to obtain satisfactory signal-to-noise ratio. Typical measurements were performed over 1.6 ns with 400 data points and a smallest increment of 20 fs close to time zero. The fluence on the cells was kept low, typically at 400 $\mu J\ cm^{-2}$. Samples were prepared in a similar way to devices, omitting the scattering layer and filled with acetonitrile. They were excited from the counter-electrode side of the device.

4.6. Nanosecond Transient Absorbance Spectroscopy (TAS). TAS was applied to the same samples than for femtosecond measurements either with acetonitrile or the desired electrolyte. Excitation (λ = 535 nm, 7 ns pulse duration, 20 Hz repetition rate) was carried out by a Powerlite 7030 frequency-doubled Q−switched Nd:YAG laser (Continuum) pumping an optical parametric oscillator (OPO, GWU-355). A planoconcave lens expanded the laser beam output to homogeneously irradiate the sample and the laser fluence was attenuated with neutral density gray filters down to <50 $\mu J\ cm^{-2}$ per pulse. The probe light was produced by a continuous wave xenon arc lamp, first passed through bandpass filters up to 1000 nm, focused onto the sample, and then through a monochromator (LOT-Oriel, Omni-λ 150), before being detected by a fast InGaAs diode (Thorlabs, SM05PD5a) across a 1 kΩ load. Data waves were recorded on a digital oscilloscope (Tektronix, DPO 7254). Satisfactory signal-to-noise ratios were typically obtained by averaging over 1000 laser shots.

■ ASSOCIATED CONTENT

Supporting Information

Synthetic procedures and characterization data of all new compounds. Details for all physical characterizations. This material is available free of charge via the Internet at http://pubs.acs.org.

■ AUTHOR INFORMATION

Corresponding Authors

jlhua@ecust.edu.cn
shaik.zakeer@epfl.ch
michael.graetzel@epfl.ch

Notes

The authors declare no competing financial interest.

■ ACKNOWLEDGMENTS

This work was supported by NSFC/China (2116110444, 21172073, 91233207 and 21372082), the National Basic Research 973 Program (2013CB733700), and the Fundamental Research Funds for the Central Universities (WJ0913001). PG is gratefully acknowledges financial support from the Swiss confederation under Swiss Government Scholarship programme and UGC, India. MG thanks the Swiss National Science Foundation and European Research Council (ERC) for an Advanced Research Grant (No. 247404) funded under the CE-Mesolight project. Yang would like to thank the funding of the visiting program, which is supported by China Scholarship Council (CSC) and Dr. Kuan-Lin Wu (National Tsing Hua University, Taiwan) for fruitful discussion.

■ REFERENCES

(1) O'Regan, B.; Grätzel, M. *Nature* **1991**, *353*, 737.
(2) Grätzel, M. *Acc. Chem. Res.* **2009**, *42*, 1788.
(3) Hagfeldt, A.; Boschloo, G.; Sun, L. C.; Kloo, L.; Pettersson, H. *Chem. Rev.* **2010**, *110*, 6595.
(4) Komiya, R.; Fukui, A.; Murofushi, N.; Koide, N.; Yamanaka, R.; Katayama, H. *Technical Digest, 21st International Photovoltaic Science and Engineering Conference, Fukuoka* **November** 2011, 2 C-50-08.
(5) Chen, C. Y.; Wang, M. K.; Li, J. Y.; Pootrakulchote, N.; Alibabaei, L.; Ngoc-le, C.; Decoppet, J. D.; Tsai, J. H.; Grätzel, C.; Wu, C. G.; Zakeeruddin, S. M.; Grätzel, M. *ACS Nano* **2009**, *3*, 3103.
(6) Gao, F. F.; Wang, Y.; Shi, D.; Zhang, J.; Wang, M. K.; Jing, X. Y.; Humphry-Baker, R.; Wang, P.; Zakeeruddin, S. M.; Grätzel, M. *J. Am. Chem. Soc.* **2008**, *130*, 10720.
(7) Yu, Q.; Wang, Y.; Yi, Z.; Zu, N.; Zhang, J.; Zhang, M.; Wang, P. *ACS Nano* **2010**, *4*, 6032.
(8) Qu, S. Y.; Hua, J. L.; Tian, H. *Sci. China Chem.* **2012**, *55*, 677.
(9) Yang, J. B.; Guo, F. L.; Hua, J. L.; Li, X.; Wu, W. J.; Qu, Y.; Tian, H. *J. Mater. Chem.* **2012**, *22*, 24356.
(10) Wu, Y. Z.; Marszalek, M.; Zakeeruddin, S. M.; Zhang, Q.; Tian, H.; Grätzel, M.; Zhu, W. H. *Energy Environ. Sci.* **2012**, *5*, 8261.
(11) Bessho, T.; Zakeeruddin, S. M.; Yeh, C.-Y.; Diau, E. W-G.; Grätzel, M. *Angew. Chim. Int. Ed.* **2010**, *49*, 6646.
(12) Marszalek, M.; Nagane, S.; Ichake, A.; Humphry-Baker, R.; Paul, V.; Zakeeruddin, S. M.; Grätzel, M. *RSC Adv.* **2013**, *3*, 7921.
(13) Mao, J. Y.; He, N. N.; Ning, Z. J.; Zhang, Q.; Guo, F. L.; Chen, L.; Wu, W. J.; Hua, J. L.; Tian, H. *Angew. Chim. Int. Ed.* **2013**, *51*, 9873.
(14) Hong, Y. P.; Liao, J.-Y.; Cao, D. R.; Zang, X. F.; Kuang, D.-B.; Wang, L. Y.; Meier, H.; Su, C.-Y. *J. Org. Chem.* **2011**, *76*, 8015.
(15) Haid, S.; Marszalek, M.; Mishra, A.; Wielopolski, M.; Teuscher, J.; Moser, J.-E.; Humphry-Baker, R.; Zakeeruddin, S. M.; Grätzel, M.; Bäuerle, P. *Adv. Funct. Mater.* **2012**, *22*, 1291.
(16) Qu, S. Y.; Wu, W. J.; Hua, J. L.; Kong, C.; Long, Y. T.; Tian, H. *J. Phys. Chem. C* **2010**, *114*, 1343.
(17) Qu, S. Y.; Qin, C. J.; Islam, A.; Wu, Y. Z.; Zhu, W. H.; Hua, J. L.; Tian, H.; Han, L. Y. *Chem. Commun.* **2012**, *48*, 6972.
(18) Holcombe, T. W.; Yum, J.-H.; Yoon, J.; Gao, P.; Marszalek, M.; Di Censo, D.; Rakstys, K.; Nazeeruddin, M. K.; Grätzel, M. *Chem. Commun.* **2012**, *48*, 10724.
(19) Yum, J.-H.; Holcombe, T. W.; Kim, Y. J.; Rakstys, K.; Moehl, T.; Teuscher, J.; Delcamp, J. H.; Nazeeruddin, M. K.; Grätzel, M. *Scientific Reports* 2014, *3*, DOI: 10.1038/srep02446.
(20) He, J. X.; Wu, W. J.; Hua, J. L.; Jiang, Y. H.; Qu, S. Y.; Li, J.; Long, Y. T.; Tian, H. *J. Mater. Chem.* **2011**, *21*, 6054.
(21) He, J. X.; Guo, F. L.; Wu, W. J.; Li, X.; Yang, J. B.; Hua, J. L. *Chem.—Eur. J.* **2012**, *18*, 7903.
(22) Ying, W. J.; Guo, F. L.; Li, J.; Zhang, Q.; Wu, W. J.; Tian, H.; Hua, J. L. *ACS Appl. Mater. Interfaces* **2012**, *4*, 4215.
(23) Zhu, W. H.; Wu, Y. Z.; Wang, S. T.; Li, W. Q.; Li, X.; Chen, J.; Wang, Z. S.; Tian, H. *Adv. Funct. Mater.* **2011**, *21*, 756.
(24) Mao, J. Y.; Guo, F. L.; Ying, W. J.; Wu, W. J.; Li, J.; Hua, J. L. *Chem. Asian J.* **2012**, *7*, 982.
(25) Chang, D. W.; Lee, H. J.; Kim, J. H.; Park, S. Y.; Park, S.-M.; Dai, L. M.; Baek, J.-B. *Org. Lett.* **2011**, *13*, 3880.
(26) Pei, K.; Wu, Y. Z.; Zhang, Q.; Chen, B.; Tian, H.; Zhu, W. H. *Chem.—Eur. J.* **2012**, *18*, 8190.
(27) Pei, K.; Wu, Y. Z.; Islam, A.; Zhang, Q.; Han, L. Y.; Tian, H.; Zhu, W. H. *ACS Appl. Mater. Interfaces* **2013**, *5*, 4986.
(28) Yella, A.; Lee, H. W.; Tsao, H. N.; Yi, C. Y.; Chandiran, A. K.; Nazeeruddin, M. K.; Diau, E. W. G.; Yeh, C. Y.; Zakeeruddin, S. M.; Grätzel, M. *Science* **2011**, *334*, 629.
(29) Yum, J.-H.; Baranoff, E.; Kessler, F.; Moehl, T.; Ahmad, S.; Bessho, T.; Marchioro, A.; Ghadiri, E.; Moser, J.-E.; Yi, C. Y.; Nazeeruddin, M. K.; Grätzel, M. *Nat. Commun.* **2012**, *3*, 631.
(30) DeVries, M. J.; Pellin, M. J.; Hupp, J. T. *Langmuir* **2010**, *26*, 9082.
(31) Sapp, S. A.; Elliott, C. M.; Contado, C.; Caramori, S.; Bignozzi, C. A. *J. Am. Chem. Soc.* **2002**, *124*, 11215.
(32) Feldt, S. M.; Gibson, E. A.; Gabrielsson, E.; Sun, L. C.; Boschloo, G.; Hagfeldt, A. *J. Am. Chem. Soc.* **2010**, *132*, 16714.
(33) Gao, P.; Kim, Y. J.; Yum, J.-H.; Holcombe, T. W.; Nazeeruddin, M. K.; Grätzel, M. *J. Mater. Chem. A* **2013**, *1*, 5535.
(34) Wang, Z. S.; Cui, Y.; Dan-oh, Y.; Kasada, C.; Shinpo, A.; Hara, K. *J. Phys. Chem. C* **2007**, *111*, 7224.
(35) Nakade, S.; Makimoto, Y.; Kubo, W.; Kitamura, T.; Wada, Y.; Yanagida, S. *J. Phys. Chem. B* **2005**, *109*, 3488.
(36) Kavan, L.; Yum, J.-H.; Grätzel, M. *Nano Lett.* **2011**, *11*, 5501.
(37) Kavan, L.; Yum, J.-H.; Nazeeruddin, M. K.; Grätzel, M. *ACS Nano* **2011**, *5*, 9171.
(38) Fabregat-Santiago, F.; Bisquert, J.; Garcia-Belmonte, G.; Boschloo, G.; Hagfeldt, A. *Sol. Energy Mater. Sol. Cells* **2005**, *87*, 117.
(39) Fabregat-Santiago, F.; Garcia-Belmonte, G.; Mora-Sero, I.; Bisquert, J. *Phys. Chem. Chem. Phys.* **2011**, *13*, 9083.
(40) Wang, M. K.; Grätzel, C.; Moon, S.; Humphry-Baker, R.; Rossier-Iten, N.; Zakeeruddin, S. M.; Grätzel, M. *Adv. Funct. Mater.* **2009**, *19*, 2163.
(41) Tsao, H. N.; Yi, C. Y.; Moehl, T.; Yum, J.-H.; Zakeeruddin, S. M.; Nazeeruddin, M. K.; Grätzel, M. *ChemSusChem* **2011**, *4*, 591.
(42) Wenger, B.; Grätzel, M.; Moser, J.-E. *J. Am. Chem. Soc.* **2005**, *127*, 12150.
(43) Ziolek, M.; Martín, C.; Sun, L. C.; Douhal, A. *J. Phys. Chem. C* **2012**, *116*, 26227.
(44) Rothenberger, G.; Fitzmaurice, D.; Grätzel, M. *J. Phys. Chem.* **1992**, *96*, 5983.
(45) Zhang, Z.; Ito, S.; Moser, J.-E.; Zakeeruddin, S. M.; Grätzel, M. *ChemPhysChem* **2009**, *10*, 1834.
(46) Li, F.; Jennings, J. R.; Wang, Q. *ACS Nano* **2013**, *7*, 8233.
(47) Wang, P.; Zakeeruddin, S. M.; Moser, J.-E.; Nazeeruddin, M. K.; Sekiguchi, T.; Grätzel, M. *Nat. Mater.* **2003**, *2*, 402.
(48) Aribia, K. B.; Moehl, T.; Zakeeruddin, S. M.; Grätzel, M. *Chem. Sci.* **2013**, *4*, 454.
(49) Wang, P.; Zakeeruddin, S. M.; Comte, P.; Charvet, R.; Humphry- Baker, R.; Grätzel, M. *J. Phys. Chem. B* **2003**, *107*, 14336.